J Mol Model (2001) 7:438–444
DOI 10.1007/s00894-001-0062-9

ORIGINAL PAPER

Joan L. Buss · Brian B. Hasinoff

A quantitative structure–activity relationship study of the rate of imide hydrolysis as a predictive model for the hydrolysis-activation of analogs of the cardioprotective agent dexrazoxane

Received: 24 July 2001 / Accepted: 22 October 2001 / Published online: 7 December 2001

Abstract The doxorubicin antioxidant cardioprotective agent dexrazoxane is a prodrug bis(imide) analog of EDTA that is only slowly hydrolyzed at physiological pH to its active iron chelating form. The kinetics of the hydrolysis of 17 imides with a wide variety of structures were studied as a function of pH in order to determine their second order base-catalyzed hydrolysis rate constants. A QSAR analysis of the rate data was carried out using molecular descriptors from molecular mechanics and quantum mechanical energy-minimized structures in order to obtain regression equations that could accurately predict the rate of imide hydrolysis. This was done to aid in the design of an analog of dexrazoxane that could hydrolyze faster in vivo and thus should be more effective with fewer toxic side effects. The best descriptors that predicted the rate of hydrolysis included bond distances, orbital energies, and charges. Electronic supplementary material to this paper can be obtained by using the Springer LINK server located at http://dx.doi.org/10.1007/s00894-001-0062-9.

Keywords QSAR · Dexrazoxane · Imide · Hydrolysis · Kinetic

Introduction

The bisdioxopiperazine dexrazoxane (ICRF-187, Zinecard, Fig. 1) is clinically used as a cardioprotective agent in combination therapy with the antitumor anthracycline doxorubicin in the treatment of advanced breast cancer. [1, 2, 3] The dose-limiting cardiotoxicity associated with doxorubicin use is believed to be due to iron-based oxidative stress. [4, 5, 6] Dexrazoxane likely acts by hydrolyzing to species that strongly chelate iron, preventing its binding to doxorubicin, or by removing iron from its complex with doxorubicin. [7, 8] The three hydrolysis products of dexrazoxane (the two one-ring open intermediates and the two-ring open final product, ADR-925, (Fig. 1a) quickly and effectively displace iron from its complex with doxorubicin in vitro, [7, 8] and are there-

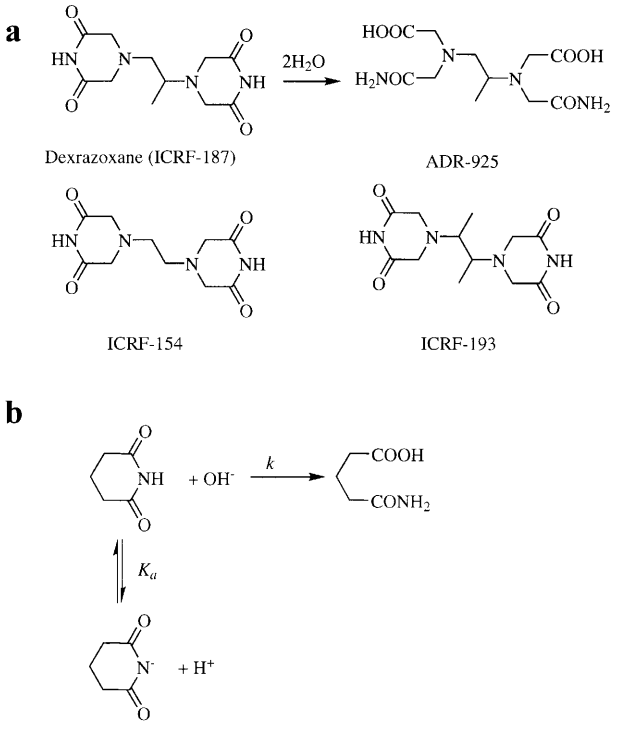

Fig. 1 **a** Structures of dexrazoxane, its two-ring opened hydrolysis product ADR-925, *meso*-ICRF-193, and ICRF-154. **b** Reaction scheme for base-catalyzed hydrolysis of non-*N*-substituted imides with glutarimide as an example. The deprotonation of the imide hydrogen in this mechanism leads to the sigmoidal pH dependence of *k* described by Eq. (3)

Electronic supplementary material to this paper can be obtained by using the Springer LINK server located at http://dx.doi.org/10.1007/s00894-001-0062-9.

J.L. Buss · B.B. Hasinoff (✉)
Faculty of Pharmacy, University of Manitoba, Winnipeg, Manitoba R3T 2N2 Canada
e-mail: B_Hasinoff@UManitoba.ca
Tel.: +1-204-474-8325, Fax: +1-204-474-7617

fore probably all pharmacologically active species. Dexrazoxane has been shown to be taken up by cells. [9] However, since the hydrolysis products of dexrazoxane are charged, they are likely trapped in cells after hydrolysis. We have recently reviewed the chemistry and biochemistry of dexrazoxane and its analogs. [10, 11]

We previously measured the ring-opening hydrolysis of dexrazoxane under a variety of conditions. The reaction is base-catalyzed and consequently is strongly pH-dependent. [12, 13, 14, 15] Even at pH 7.4 the hydrolysis is still largely base-catalyzed. [12] In Tris buffer at pH 7.4 and 37 °C the half-time for hydrolysis of dexrazoxane to its one-ring open intermediates is approximately 9 h. [13, 14] The plasma half-life of dexrazoxane in humans is 4.2 h, [16] which is much shorter than its half-life for hydrolysis under physiological conditions. As a result approximately half of the dexrazoxane administered is recovered intact in the urine. [17] Consequently, large doses of dexrazoxane, up to 1,000 mg/m^2, must be administered to maximize its cardioprotective effect, [1] although doses above 600 mg/m^2 are myelosuppressive. [16] The latter effects are likely mediated by the ability of bisdioxopiperazines to inhibit DNA topoisomerase II. [18]

An analog of dexrazoxane that hydrolyzed several times faster in vivo would presumably allow lower doses to be given, since a larger fraction of the drug would be hydrolyzed to its active forms before its excretion. Myelosuppressive effects could be reduced or eliminated. The objective of this study was to develop a quantitative structure–activity relationship of imide hydrolysis rates that could be used to design faster hydrolyzing, more effective and less toxic analogs of dexrazoxane. Simple imides with a variety of structures were chosen to model and study the kinetics so that the QSAR data obtained would have good predictive value over a range of possible design structures.

Materials and methods

Materials

Diacetamide, *N*-methyldiacetamide, *N*-methylbis(trifluorodiacetamide), succinimide, *N*-methylsuccinimide, *N*-2,6-xylylsuccinimide, maleimide, *N*-methylmaleimide, *N*-ethylmaleimide, *N*-phenylmaleimide, *N*-4-chlorophenylmaleimide, *N*-3,4-xylylmaleimide, phthalimide, adipimide, and glutarimide were obtained from Aldrich (Milwaukee, Wisc.). ICRF-154 and *meso*-ICRF-193 (Fig. 1a) were prepared essentially as described. [19] Dexrazoxane was a gift from Adria Laboratories (Columbus, Ohio). Optical grade KCl (Aldrich) of low UV absorbance was used to minimize the background absorbance at the low wavelengths at which the reactions were followed.

Kinetic analysis

The kinetics of imide hydrolysis were followed spectrophotometrically in 1 cm stoppered silica cells on a Cary 1 spectrophotometer (Varian, Mulgrave, Australia) at 25 °C in a thermostated cell compartment in 50 mM ammonia buffer and potassium hydroxide solutions over a pH range of approximately 8 to 13.2. The total ionic strength was maintained at 150 mM with KCl. Below pH 11.1, reactions were carried out in ammonia/KCl buffer, and the pH was measured immediately following each experiment. Above pH 11.1, reactions were carried out in KOH/KCl solutions, and the pH was calculated from the analytical concentration of KOH. Stock solutions of the imides were made in ethanol or DMSO, such that the final concentrations of the imide and co-solvent were 100 μM and less than 1%, respectively. Reactions were initiated by the addition of imide to the spectrophotometer cell. Data were analyzed using Cary 1/3E software (Varian) and SigmaPlot 5.0 for DOS (Jandel Scientific, San Rafael, Calif.).

Molecular mechanics optimizations

Molecular mechanics calculations using the MMX algorithm, which is based on the MM2 algorithm, [20] were carried out using PCModel version 4.0 for DOS (Serena Software, Bloomington, Ind.). Minimizations were repeated at least three times, until the energies no longer significantly decreased. Aromatic rings, and the carbon, oxygen, and nitrogen atoms of the imide functional group were modeled as π-atoms, and minimization was performed using restricted Hartree–Fock self-consistent field calculations. Optimized structures of the tetrahedral hydrolysis intermediates, modeled as mono-anions, as was done in previous studies of esters [21] and lactams, [22] were generated using the corresponding minimized imide structures as starting points, and were minimized at least three times, until the total energy no longer significantly decreased.

AM1 quantum mechanical optimizations

The MMX-optimized structures were used as starting points for the semiempirical quantum mechanical (AM1, using Hyperchem release 4 for Windows, Hypercube Inc., Gainesville, Fla.) optimizations. Structures were minimized in vacuo, using a restricted Hartree–Fock self-consistent field. Optimization proceeded by a Polak–Ribiere algorithm. Since minimization until the gradient was less than either 0.01 or 0.1 kcal Å^{-1} yielded energies which differed only in the seventh significant figure, the cutoff for structure optimization was set at a gradient of 0.1 kcal Å^{-1}.

QSAR analysis

Regression analyses were done using SigmaStat (version 1 for DOS, Jandel Scientific, San Rafael, Calif.). Correlation of individual independent variables was deter-

mined using the Pearson product moment correlation coefficient. The best subsets algorithm in this software was used to identify pairs of variables as candidates for multiple linear regression analysis. Constant variance was tested by the Spearman rank correlation coefficient (p=0.05). Normality of the residuals was tested by the Kolmogorov–Smirnov test (p=0.05). The significance of each independent variable was examined using the F statistic (F=4) in a stepwise regression in which the independent variable with the higher F value was entered into the equation first. The residuals were examined with respect to each independent variable and the dependent variable for trends and outliers. Where there were like measurements on the structures (e.g. two carbonyl carbon–oxygen bond distances) an average of the like measurements was used in the QSAR analysis. All errors quoted are SEMs (standard error of the mean).

Results

Kinetic results: *N*-substituted imides

The hydrolysis of imides was followed by UV spectrophotometry at their absorption maxima, which varied from 210 to 265 nm. Typical absorbance–time data for *N*-methylmaleimide obtained at different pH values are shown in Fig. 2a as an example. These data were cleanly fitted to a three-parameter equation for an exponential decay:

$$A = A_0 e^{-k_{obs}t} + A_\infty \quad (1)$$

in which A and A_∞ are the absorbances at time t and infinity, respectively, k_{obs} is the pseudo-first-order rate constant, and A_0 is the amplitude of the absorbance change. For all the imides except *N*-methylsuccinimide the parameter k_{obs} varied linearly with hydroxide ion concentration. Representative kinetic data for *N*-methylmaleimide are shown on a log–log plot in Fig. 2b. The plot has a linear-least squares calculated slope of 1.12±0.05, indicating that the hydrolysis reaction is first-order in hydroxide ion concentration. Thus, the data (weighted assuming the standard errors in k_{obs} were proportional to k_{obs}) were fitted to a linear equation:

$$k_{obs} = k\left[OH^-\right] \quad (2)$$

in which k is a second-order rate constant for base-catalyzed hydrolysis (Table 1). The addition of a constant term to this equation, corresponding to a contribution to k_{obs} from water-catalyzed hydrolysis, did not significantly improve the fits. Only for *N*-methylsuccinimide was it necessary to add a quadratic term, $k_q[OH^-]^2$, to Eq. (2), which gave a value of k_q of 6900±1400 M^{-2} min^{-1}.

Kinetic results: non-*N*-substituted imides

Similar to the *N*-substituted imides, non-*N*-substituted imides had a characteristic absorbance peak at approximately 210 nm, as has been shown for dexrazoxane. [12, 13, 14] At a pH near 10, the imide proton dissociates, causing a shift of this peak to a longer wavelength. The maximum absorbance of the deprotonated imide occurs at 227 nm for dexrazoxane. [12, 13, 14] The hydrolysis of the non-*N*-substituted imides was followed by observing the decrease in the absorbance of the imide anion peak at wavelengths from 217 to 240 nm which, at constant pH, is proportional to the total concentration of imide. Absorbance–time data for diacetamide, succinimide,

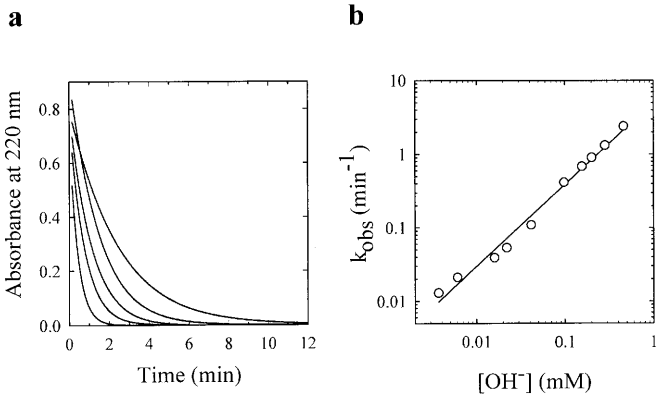

Fig. 2 **a** The change in absorbance with time for the hydrolysis of *N*-methylmaleimide, measured spectrophotometrically at 220 nm. Measurements were made at 25 °C in ammonia buffer, at pH values of 9.99, 10.19, 10.30, 10.45, and 10.66 (in order of decreasing half-time). The ionic strength was maintained at 150 mM. **b** Hydroxide ion-dependence of the hydrolysis of *N*-methylmaleimide plotted on a log–log scale. The line is linear-least squares calculated with a slope of 1.12±0.05 and an r^2 of 0.987

Table 1 Second order rate constants k for the base-catalyzed hydrolysis of various imides and their kinetically determined pK_a values at 25 °C and ionic strength 0.150 M

Imide	k (M^{-1} min^{-1})	pK_a [a]
Diacetamide	65.0±0.2	12.77±0.01
N-Methyldiacetamide	77±5	–
N-Methylbis(trifluorodiacetamide)	42±2	–
Succinimide	5.5±0.9	10.86±0.08
N-Methylsuccinimide	14±4	–
N-2,6-Xylylsuccinimide	31±1	–
Maleimide	1690±200	10.41±0.06
N-Methylmaleimide	3230±300	–
N-Ethylmaleimide	1440±200	–
N-Phenylmaleimide	10560±200	–
N-3,4-Xylylmaleimide	7270±100	–
N-4-Chlorophenylmaleimide	16700±300	–
Phthalimide	560±3	10.08±0.06
Adipimide	150±3	11.41±0.05
Glutarimide	91±8	12.01±0.05
ICRF-154	125±20	10.10±0.09
ICRF-193	220±30	10.41±0.07
Dexrazoxane[b]	51±6	10.47±0.06

[a] Calculated from a fit of the kinetic data to Eq. (3) for non-*N*-substituted imides. All errors are standard errors of the mean from non-linear least squares curve fitting

[b] Since dexrazoxane is asymmetrical, the rate constant measured is the sum of the individual ring-opening rate constants

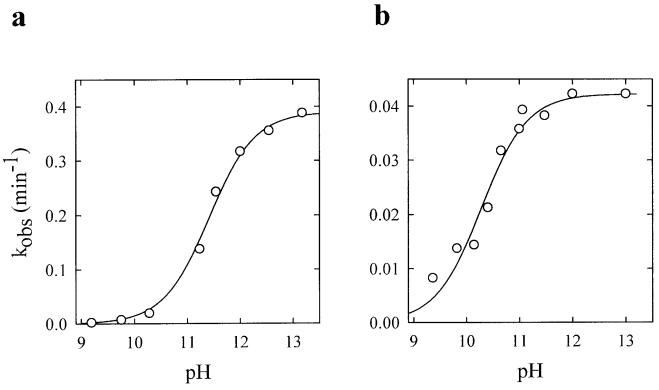

Fig. 3a,b pH dependence of the pseudo-first order rate constant of hydrolysis k_{obs} of **a** ICRF-193 and **b** adipimide, measured at 240 and 239 nm, respectively. The curves are calculated from non-linear-least squares fits of the k_{obs} data to Eq. (3) and yield pK_a values of 10.41±0.07 and 11.41±0.05, respectively

adipimide, phthalimide, adipimide, and glutarimide were collected as for the *N*-substituted imides, and fitted to Eq. (1). Complete hydrolysis of ICRF-154 and ICRF-193 (Fig. 1a) must necessarily involve two steps, since these compounds have two imide groups. To isolate the first hydrolysis step, initial rate data (corresponding to less than 10% of the total change in absorbance) were collected and analyzed for these imides. Succinimide was also analyzed by this method due to its slow hydrolysis. The pseudo-first-order rate constants were calculated from the slopes of the plots and the absorbances of the imides and their final hydrolysis products.

The values of k_{obs} were observed to increase sigmoidally with pH with an inflection point corresponding to the pK_a of the imide functional group. It has previously been shown for maleimide, [23] succinimide, [24] and ethosuximide [25] that the imide anion, which is less electrophilic than the neutral protonated species, is resistant to nucleophilic attack by hydroxide ion in the pH range of interest in this study. These data were fitted to the following equation, which describes hydroxide-ion-catalyzed hydrolysis in which only the neutral protonated imide species is hydrolyzed (Fig. 1b):

$$k_{obs} = \frac{k\left[OH^-\right]}{K_a/\left[H^+\right] + 1} \quad (3)$$

in which K_a is the acid dissociation constant for the imide proton, and k is the second-order base-catalyzed hydrolysis rate constant. As the pH increases the concentration of the reactive neutral imide species decreases while the concentration of the reactive OH^- species increases, leading to the resulting sigmoidal pH dependence. Representative data for the pH dependence of ICRF-193 and adipimide hydrolysis are shown in Fig. 3a and b, respectively. Values of k and pK_a obtained from a three-parameter non-linear least squares fits of the k_{obs} data to Eq. (3) are given in Table 1. The addition of an additional constant term to the numerator, corresponding to a contribution to k_{obs} from nucleophilic attack by water, did not significantly improve the fits.

Mechanism of imide hydrolysis

Imides are thought to hydrolyze via a $B_{AC}2$ mechanism, as do esters and amides. [26] The mechanism likely involves nucleophilic attack of hydroxide ion at the carbonyl carbon atom forming a tetrahedral intermediate, which subsequently collapses to the products, a carboxylate and an amide. Hydrolysis rates of imides likely depend on both geometric and electronic factors, which determine their reactivities toward hydroxide ion. Since hydrolysis begins with nucleophilic attack by OH^- on the carbonyl carbon atom, the environment of this atom is likely important. Thus, atomic charges, bond lengths and angles, and torsion angles may be useful predictors of imide hydrolysis. Since the lowest unoccupied molecular orbital (LUMO) of the imide accepts electrons from the nucleophile, its energy might also reasonably be expected to be inversely correlated to hydrolysis rate. The most useful information regarding imide hydrolysis rates should come from analysis of the rate-determining step. However, there is disagreement over whether it is the formation or the collapse of the tetrahedral intermediate that is rate-determining. [23, 27, 28, 29] Thus, both the imides and their corresponding tetrahedral intermediates were modeled, and descriptors were extracted from both series of structures for analysis.

Molecular modeling

For diacetamide, [30] *N*-methylbis(trifluorodiacetamide), [31] succinimide, [32] *N*-ethylmaleimide, [33] phthalimide, [34] glutarimide, [35] and ICRF-154 [36] the crystal structures are known, and thus their X-ray coordinates were used as starting points for structure optimization. The starting structures for *N*-methyldiacetamide, the substituted succinimides, the remaining maleimides, and ICRF-193 were obtained by modification of the crystal structures of *N*-methylbis(trifluorodiacetamide), succinimide, *N*-ethylmaleimide, and ICRF-154, respectively. Due to the conformational flexibility of the seven-membered ring in adipimide, two energy minima were found for adipimide. The lowest-energy conformation obtained from the MMX optimization had both sp^3 carbon atoms on the same side of the imide plane (as defined by the imide carbonyl groups), while that obtained from the AM1 optimization had these atoms on opposite sides of the plane. Since it was expected that the AM1 results might be more useful for the QSAR analysis, due to their better approximations of electronic measurements, the latter conformation was used in the analysis. The diacetamides were minimized from three starting structures, corresponding to the *E,E*, *E,Z*, and *Z,Z* conformations. The bisdioxopiperazines, which also have conformational flexibility, were minimized from various starting

structures with torsion angles of the main chain carbon–carbon bonds rotated 0, 120 and 240° from those obtained from the minimization of the crystal structure of ICRF-154. The X-ray crystal structures of diacetamide, succinimide, *N*-ethylmaleimide, phthalimide, and glutarimide were compared to the MMX- and AM1-optimized structures and at maximum the root-mean-square difference in atomic positions was 0.13 Å.

Due to the geometric restrictions of cyclic molecules, and to the stabilization of the imide functional group by electron delocalization, the optimized imide structures tended toward planarity. Thus, the succinimides, maleimides, and phthalimide had nearly planar conformations. Glutarimide and the bisdioxopiperazines, which have six-membered rings, preferred a half-chair conformation, which permitted a planar conformation of the imide group. Although *N*-methyldiacetamide and *N*-methylbis(trifluorodiacetamide) preferred an *E,E* conformation, diacetamide, which has no bulky *N*-substituent, preferred an *E,Z* conformation.

The tetrahedral hydrolysis intermediates of the five- and six-membered imides preferred envelope and cyclohexene-like conformations, respectively, which retained a planar arrangement of the remaining sp^2 centers. The C_α–$C_{carbonyl}$–N angles decreased, corresponding to the shift from sp^2 to sp^3 hybridization. The species with five-membered rings had angles ranging from 100 to 104°, reflecting the ring strain due to the remaining sp^2 centers, while the other species had angles from 110 to 114°, consistent with sp^3 hybridization. The C–N bond length increased to 1.44–1.49 Å, due to the loss of π character.

A total of 63 basic descriptors which measured electronic and geometric properties were derived from the MMX- and AM1-optimized structures of the imides and their tetrahedral intermediates. These descriptors included measures for the atoms likely involved in hydrolysis, such as partial charges, bond lengths, and bond and torsion angles, as well as descriptors which measured properties of the entire molecule, including orbital energies calculated by the AM1 algorithm and the individual terms used in the calculation of the total energy of the system by the MMX algorithm. Forty-eight additional descriptors were derived from these basic descriptors by simple transformations. Examples included squares and absolute values of individual descriptors, sums and differences of pairs of descriptors, and squares of differences between measurements from the imides, subtracted from that of diacetamide, which likely represents a relatively unstrained system.

QSAR analysis

Single variable regression analysis of the individual descriptors with log *k* as the dependent variable was carried out to identify the best individual descriptors. The best individual descriptors were those which measured both electronic and geometric parameters and all but one was obtained using the AM1 algorithm. The five best individual descriptors obtained were:

- *RCC*: length (Å) of the $C_{tetrahedral}$–C_α bond of the tetrahedral intermediate, measured on the structures optimized by the MMX algorithm (r^2=0.771, p<0.001)
- *LUMO2*: square of the lowest unoccupied molecular orbital of the imide (eV^2), measured on the structures optimized by the AM1 algorithm (r^2=0.743, p<0.001)
- *HOLU*: difference between the highest occupied and lowest unoccupied molecular orbitals of the imide (eV), measured on the structures optimized by the AM1 algorithm (r^2=0.722, p<0.001)
- *RCN2*: square of the difference in the average $C_{carbonyl}$–N_{imide} bond lengths ($Å^2$) between each imide and diacetamide, measured on the structures optimized by the AM1 algorithm (r^2=0.717, p<0.001)
- *LUMO*: lowest unoccupied molecular orbital of the imide (eV), measured on the structures optimized by the AM1 algorithm (r^2=0.646, p<0.001)

Since residual analysis of the individual descriptors determined that none of the imides in the data set had values of *k* which were consistently poorly predicted, it was concluded that the data set was homogeneous, and that the structural factors determining imide hydrolysis rates were the same for all members of the data set.

In order to refine the QSAR further, multiple linear regression analysis was undertaken to determine whether equations containing two descriptors had an improved ability to predict log *k*. Dexrazoxane (Fig. 1a) itself was not included in the data set because it is unsymmetrical and the two rings open at different rates. [13, 14] A best subsets algorithm was used to identify pairs of variables as candidates for multiple linear regression analysis. The equations that met all statistical conditions as described in the Materials and methods section were ranked by r^2. A search for regression equations with three or more variables was not undertaken, as the contributions of additional variables were not significant, as measured by the *F* statistic.

The ten best equations had values of r^2 that varied from 0.912 to 0.859. Eight of these equations contained the variable *RCC*, which was also the best single descriptor, as described above. The second variable in these equations was usually an electronic parameter, such as an atomic charge calculated from the AM1 algorithm. The remaining two equations contained the variable *LUMO2*. The best equation overall (along with the standard error of the estimate, *s*), which contained the variable *RCC*, and the best equation containing *LUMO2* were, respectively:

$$\log k = 101.812 - 60.4041\,(RCC) - 10.1978\,(ZCN)$$
$$r^2 = 0.912, pZZZ38; lt; 0.001, s = 0.329 \quad (4)$$

$$\log k = 1.15776 + 2.5015\,(LUMO2) - 23.6256\,(ZCO)$$
$$r^2 = 0.864, pZZZ38; lt; 0.001, s = 0.410 \quad (5)$$

in which *ZCN* and *ZCO* are defined as follows:

Table 2 Calculated and experimental values of log *k* for base-catalyzed imide hydrolysis

Imide	log *k* (Eq. 4)	log *k* (Eq. 5)	log *k* (experimental)
Diacetamide	1.72	2.28	1.81
N-Methyldiacetamide	1.92	2.23	1.89
N-Methylbis(trifluorodiacetamide)	1.31	1.84	1.62
Succinimide	1.17	1.40	0.74
N-Methylsuccinimide	1.59	1.51	1.15
N-2,6-Xylylsuccinimide	1.78	0.98	1.49
Maleimide	3.03	3.75	3.23
N-Methylmaleimide	3.52	3.35	3.51
N-Ethylmaleimide	3.63	3.18	3.16
N-Phenylmaleimide	3.92	3.60	4.02
N-3,4-Xylyl maleimide	3.90	4.34	4.22
N-4-Chlorophenylmaleimide	3.94	3.38	3.86
Phthalimide	2.88	2.81	2.75
Adipimide	1.52	1.86	2.18
Glutarimide	1.99	1.85	1.96
ICRF-154	2.18	1.77	2.10
ICRF-193	2.01	1.91	2.34
3-Methylglutarimide	1.57	1.87	1.60[a]
4-Methyl-2,6-dioxopiperazine	1.67	1.56	2.41[a]

[a] [37, 38]

- *ZCN*: difference of the average charges of the $C_{carbonyl}$ and N_{imide} of the imide, measured on the structure optimized by the AM1 algorithm
- *ZCO*: sum of the average charges of the carbonyl group of the imide, measured on the structure optimized by the AM1 algorithm

The values of r^2=0.912 and 0.864 for Eqs. (4) and (5), respectively, and their associated *p* of less than 0.001 are indicative of the high predictive power of these models. The values of log *k* calculated for each imide from these equations are compared with the experimental values in Table 2. Overall, these equations successfully predicted log *k* for the whole series of imides investigated.

The second order rate constants *k* for hydrolysis of 3-methylglutarimide and 4-methyl-2,6-dioxopiperazine have been measured [37, 38] at the same temperature as this study, but at an ionic strength of 0.5 M. As a test of their predictive value, Eqs. (4) and (5) were used to calculate log *k* for these imides. Calculated and experimental values are given in Table 2. Both equations predicted log *k* well for 3-methylglutarimide, while predictions for 4-methyl-2,6-dioxopiperazine were low. The latter result is somewhat surprising, given the agreement of the predicted and experimental values of log *k* for ICRF-154 and ICRF-193 (Fig. 1a), which are structurally analogous to 4-methyl-2,6-dioxopiperazine.

Discussion

The ring-opening hydrolysis of dexrazoxane is base-catalyzed, which results in its strong pH-dependence. [12, 13, 14, 15] We have shown [12] that even at pH 7.4 the hydrolysis is still largely base-catalyzed. Thus, our measurements, which were carried out at pH values higher than this, should be good predictors of hydrolysis rates at physiological pH.

The small difference between the rates of diacetamide and glutarimide base-catalyzed hydrolysis is likely due to the steric effects of the bridging methylene group of glutarimide, which likely causes a modest destabilization. The *k* for base-catalyzed hydrolysis for adipimide was 1.7 times that of glutarimide, consistent with the usual observation that stability decreases with ring size. In agreement with previous predictions that five-membered rings are more stable than their six-membered analogs, [39] the *k* for succinimide was approximately 17 and 12 times lower than those for glutarimide and diacetamide, respectively. A previous study reported a ten-fold decrease in the hydrolysis rate of *N*-methylsuccinimide relative to *N*-methyldiacetamide, [40] which is in good agreement with the six-fold difference observed in this study. Maleimide hydrolyzed 300 times faster than its saturated analog, succinimide. Although the overall geometry of these imides is similar, it would be expected that maleimide has additional ring strain, both due to the rigidity required for maximal electron delocalization of the ring, and to the larger number of in-plane steric interactions in maleimide.

The bisdioxopiperazines have similar values of *k* and pK_a, indicating that the presence of methyl groups on the alkyl chain joining the two imide rings has little influence on the lability of the imide functional group, as previously observed for a series of bisdioxopiperazines. [15] The pK_a of glutarimide, however, is much higher than those of the bisdioxopiperazines, due to the absence of the electron-withdrawing tertiary nitrogen atom.

The best single descriptors of imide hydrolysis included measurements of electronic properties primarily based on the energy of the lowest unoccupied molecular orbital of the imides, which would be expected to correlate with hydrolysis rates, since it is this orbital which will accept the electron pair from the incoming nucleophilic hydroxide ion to form the tetrahedral hydrolysis intermediate. Geometric descriptors describing the bond lengths of the carbonyl carbon atom were also correlated to log *k*. Descriptors measured by both the MMX and AM1 algorithms were found to be among the best des-

criptors. The best ten equations identified by the best subsets analysis included ones with *RCC* or *LUMO2*, the two descriptors which were most highly correlated to log *k*. It is unclear why *RCC* was such a highly correlated descriptor as *RCC* measures a bond in the tetrahedral intermediate that is not being broken. It may be that the descriptor *RCC* may report structural information to the imide group from the rest of the molecule since the imide groups of all these molecules are identical.

QSAR analysis of a series of imides has identified descriptors that allow the prediction of rates of hydroxide ion-promoted hydrolysis of imides that vary in ring size and *N*-substituents. The regression equations developed here will allow the prediction of hydrolysis rates for the synthesis of dexrazoxane analogs. Dexrazoxane is slow to hydrolyze [13, 14] and thus much of it is excreted unchanged. [17] A faster-hydrolyzing analog should produce the active metal chelating form more quickly and thus be more effective and less toxic at lower doses.

Supplementary material The definitions of the descriptors extracted from molecular modeling of imides (from both MMX and AM1 algorithms) that were examined in the QSAR analysis are available as supplementary material. The values of the descriptors for each imide examined are also available as supplementary material.

Acknowledgments This work was supported by the Canadian Institutes of Health Research, the Canada Research Chairs program, and a Canada Research Chair in Drug Development for Dr. Brian Hasinoff. Joan Buss was supported by Rx&D/Canadian Institutes of Health Research and Manitoba Health Research Council studentships.

References

1. Speyer JL, Green MD, Zeleniuch-Jacquotte A, Wernz JC, Rey M, Sanger J, Kramer E, Ferrans V, Hochster H, Meyers M, Blum RH, Feit F, Attubato M, Burrows W, Muggia FM (1992) J Clin Oncol 10:117–127
2. Swain SM, Whaley FS, Gerber MC, Weisberg S, York M, Spicer D, Jones SE, Wadler S, Desai A, Vogel C, Speyer J, Mittelman A, Reddy S, Pendergrass K, Velez-Garcia E, Ewer MS, Bianchine JR, Gams RA (1997) J Clin Oncol 15:1318–1332
3. Swain SM, Whaley F, Gerber MC, Ewer MS, Bianchine JR, Gams RA (1997) J Clin Oncol 15:1333–1340
4. Gianni L, Corden BJ, Myers CE (1983) Rev Biochem Toxicol 5:1–82
5. Myers CE, Gianni L, Simone CB, Klecker R, Greene R (1982) Biochemistry 21:1707–1713
6. Malisza KL, Hasinoff BB (1995) Arch Biochem Biophys 321:51–60
7. Hasinoff BB (1989) Agents Actions 26:378–385
8. Buss JL, Hasinoff BB (1993) Agents Actions 40:86–95
9. Dawson KM (1975) Biochem Pharmacol 24:2249–2253
10. Hasinoff BB (1998) Semin Oncol 25 [Suppl 10]:3–9
11. Hasinoff BB, Hellmann K, Herman EH, Ferrans VJ (1998) Curr Med Chem 5:1–28
12. Hasinoff BB (1990) Drug Metab Dispos 18:344–349
13. Hasinoff BB (1994) J Pharm Sci 83:64–67
14. Hasinoff BB (1994) Int J Pharm 107:67–76
15. Herman EH, Zhang J, Hasinoff BB, Chadwick D, Clark JRJ, Ferrans VJ (1997) Cancer Chemother Pharmacol 40:400–408
16. Hochster H, Liebes L, Wadler S, Oratz R, Wernz JC, Meyers M, Green M, Blum RH, Speyer JL (1992) J Natl Cancer Inst 84:1725–1730
17. Earhart RH, Tutsch KD, Koeller JM, Rodriguez R, Robins HI, Vogel CL, Davis HL, Tormey DC (1982) Cancer Res 42: 5255–5261
18. Hasinoff BB, Kuschak TI, Yalowich JC, Creighton AM (1995) Biochem Pharmacol 50:953–958
19. Creighton AM (1971) UK Patent 1,234,935
20. Burkert U, Allinger NL (1982) Molecular Mechanics, ACS Monograph 177. American Chemical Society, Washington, D.C.
21. Pranata J (1994) J Phys Chem 98:1180–1184
22. Frau J, Donoso J, Munoz F, Blanco FG (1992) J Comput Chem 13:681–692
23. Barradas RG, Fletcher S, Porter JD (1975) Bull Soc Chim Fr 54:1400–1404
24. Euler HV, Olander A (1928) Z Phys Chem 137:393–398
25. Yakatan GJ, Fan T (1977) Drug Dev Ind Pharm 3:315–338
26. Bender ML (1960) Chem Rev 60:53–113
27. Edward JT, Terry KA (1957) J Chem Soc:3527–3531
28. Khan MN, Khan AA (1975) J Org Chem 40:1793–1794
29. Machida M, Machida MI, Kanaoka Y (1977) Chem Pharm Bull 25:2739–2743
30. Matias PM, Jeffrey GA, Ruble JR (1988) Acta Crystallogr, Sect B 44:516–522
31. Rochon FD, Kong PC, Melanson R (1990) Inorg Chem 29:2708–2712
32. Mason R (1961) Acta Crystallogr, Sect B 14:720–724
33. McPhalen CA, James MNG (1983) Acta Crystallogr, Sect C 39:1441–1445
34. Ng SW (1992) Acta Crystallogr, Sect C 48:1695–1698
35. Petersen CS (1971) Acta Chem Scand 25:379–389
36. Camerman N, Hempel A, Camerman A (1984) Science 225:1165–1166
37. Sisco JM, Stella VJ (1992) Pharm Res 9:1076–1082
38. Sisco JM, Stella VJ (1992) Pharm Res 9:1209–1214
39. Brown HC, Brewster JH, Shechter H (1954) J Am Chem Soc 76:467–474
40. Hall Jr HK, Brandt MK, Mason RM (1958) J Am Chem Soc 80:6420–6427